

University of Wyoming Aeronautics Laboratory
Mechanical Engineering Department

University of Wyoming Aeronautics Laboratory
Mechanical Engineering Department
College of Engineering
University of Wyoming
PO Box 3295
Laramie, Wyoming 82071
Phone (307)766-6284
FAX (307)766-2695



UWAL-2000-01

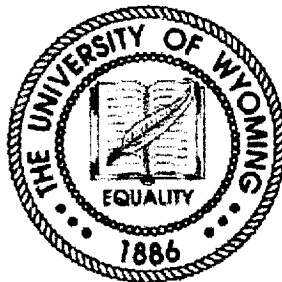
Reduction of Base Drag on Launch Vehicles

Final Report

Jonathan W. Naughton

March, 1999 through November 1999

NASA Research Grant NAG4-167



Introduction

This report describes the work accomplished during a first-year investigation of base drag reduction for launch vehicles. Interest in this work has arisen due to the large base areas associated with the current generation of launch vehicles. For example, the X-33 and Venture Star configurations all have large base areas because of the aero-spike engines they use. Because of the large base-to-wetted area ratios of these vehicles, the majority of the vehicle drag is due to base drag.

Based on previous research, there appears to be a means for reducing the base drag on such vehicles. Hoerner (1965) and Salzman (1999) have demonstrated a clear relationship between viscous fore-body drag and base drag as shown in Figure 1. The figure shows that, for subsonic flow conditions, an increase in fore-body drag causes a decrease in base drag. This base-drag reduction is a result of boundary layer effects at the base of the vehicle. The shear layer that develops from the boundary layer separating at the back of the vehicle is the conduit through which momentum is transferred from the high energy free-stream flow to the low-energy fluid in the base area. One way to think of the base drag is that it is the momentum required to accelerate this low-energy fluid. The boundary layer that develops on the fore body acts as an "insulator" between the external flow and the low-energy air at the base. As the viscous fore-body drag is increased, the boundary layer thickness at the aft end of the fore body increases, thereby reducing the rate at which momentum is transferred to the base area. As a result of the lower momentum transfer (or reduced pumping), the base pressure coefficient rises resulting in a reduction of base drag.

More significantly, the data of figure 1 shows that projectiles whose base drag coefficient is greater than 0.30 (referenced to the base area) have ratios of base drag to viscous fore-body drag that lie on the steep vertical portion of the curve. In this region, a small increment in the viscous fore-body drag should result in a relatively large decrease in the base drag. Conceptually, if the added increment in fore-body viscous drag is optimized with respect to the base drag reduction, then it may be possible to reduce the overall drag of the configuration. This optimal drag-region, or "drag bucket," is depicted in figure 2. Here the base drag and the total vehicle drag are plotted against the viscous fore-body drag along with measured data for several hypersonic lifting-body and wing-body configurations (Saltzman 1999, Whitmore & Moes 1999): X-15, M2 -F1, M2 - F2, Shuttle, HL-10, X-24A, X-24B, and the SR-71 LASRE (Taken to represent the characteristics of the X-33 / Venture-Star). Whereas the drag characteristics of most of the previously flown hypersonic shapes lie near or slightly to the right of the drag minimum, those of the X-33 lie far to the left of the drag minimum. The simple model of figure 2 is presented only as an illustration of the "drag-bucket" concept. Clearly, the fore-body pressure profile, and presence of induced drag and localized interference or flow separation drag will likely alter the shape of the "optimal" curve presented in figure 2. The challenge is to determine the fore-body drag value that produces the minimum vehicle drag in a real-world configuration.

Recent work on the LASRE flight program has demonstrated that a reduction in base drag may be accomplished by increasing fore-body drag (see Figure 1 and the paper by Whitmore & Moes 1999). In this study, a portion of the fore body of the LASRE vehicle was roughened to increase the fore-body drag. A decrease of base drag was observed at all Mach numbers (subsonic, transonic and supersonic) validating the application of this drag-reduction technique to transonic and supersonic Mach numbers. Unfortunately, the increase in fore-body drag was greater than the reduction in base drag, and thus no net drag reduction was observed. The increase in fore-body drag is due to both increased pressure drag and increased viscous drag caused by the roughened surface.

Although the data taken during the LASRE flight test was very limited, the results indicate that, over a wide range of Mach number, increasing fore-body drag reduces base drag. The goal is to produce the maximum base-drag reduction with a minimum increase in fore-body drag.

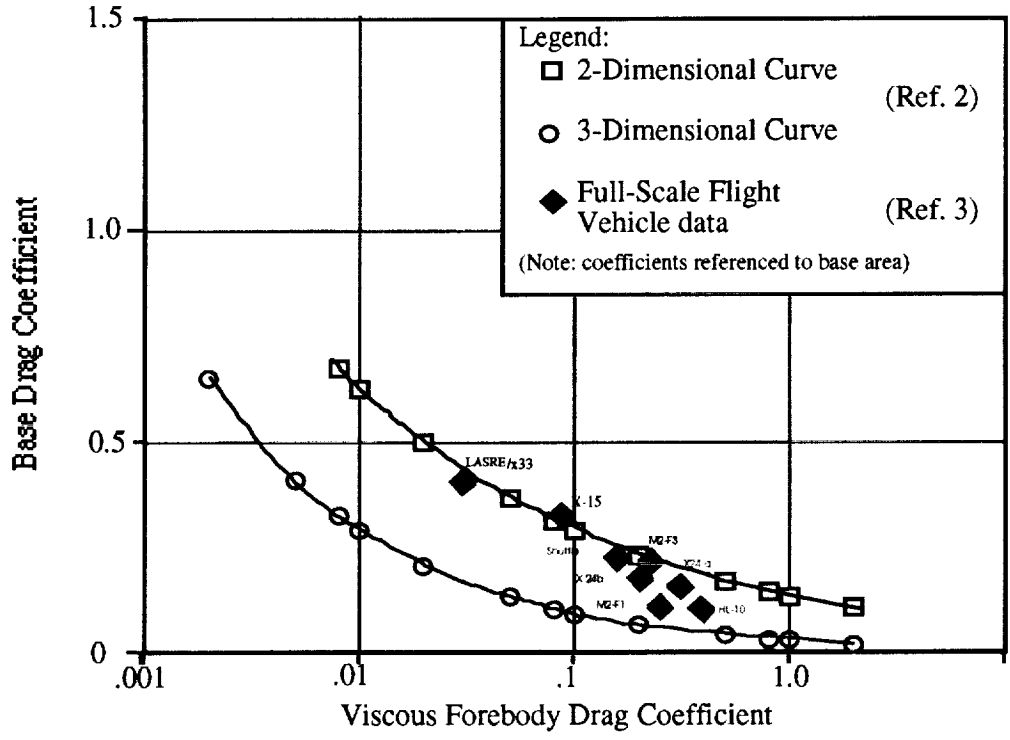


Figure 1 - Relationship between viscous forebody drag and base drag.

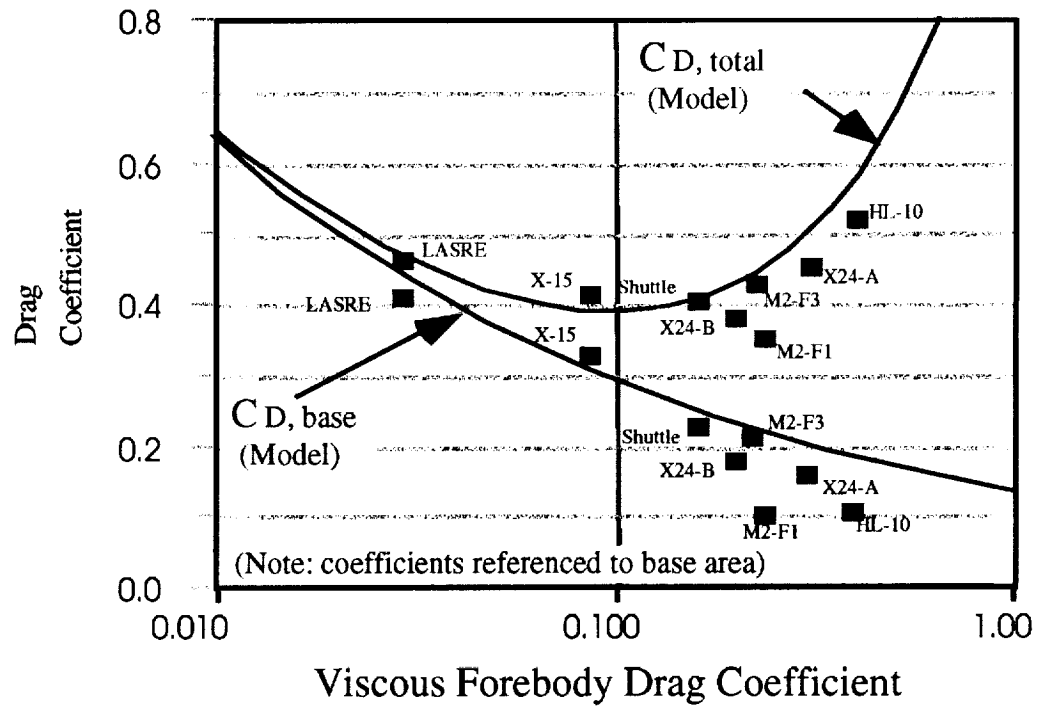


Figure 2 - Drag bucket concept.

Overall Project Goals

The goal of this project is to demonstrate the feasibility of using boundary-layer control on a large base area reentry vehicle to reduce the overall vehicle drag. To accomplish this goal, several intermediate steps must be accomplished

- A baseline set of viscous forebody drag and base drag must be developed.
- A means for measuring forebody viscous drag on smooth and rough surfaces must be demonstrated.
- The relationship for $C_{D,forebody}$ versus $C_{D,base}$ must be rigorously established over a wide range of Mach number.

Accomplishing these goals should provide enough information to establish that a net drag reduction can be achieved through the addition of viscous forebody drag. Having accomplished this, optimizing the means of introducing of additional fore-body drag and investigating how to implement it on an actual reentry vehicle may be explored.

Year 1 Goals

The goals for year 1 are listed below.

- Design and build a flat plate to investigate the measurement of skin friction on rough surfaces.
- Measure integrated skin friction on a large floating element to serve as a baseline measurement for surface shear stress on rough surfaces.
- Investigate means of measuring viscous forebody drag on smooth and rough surfaces.

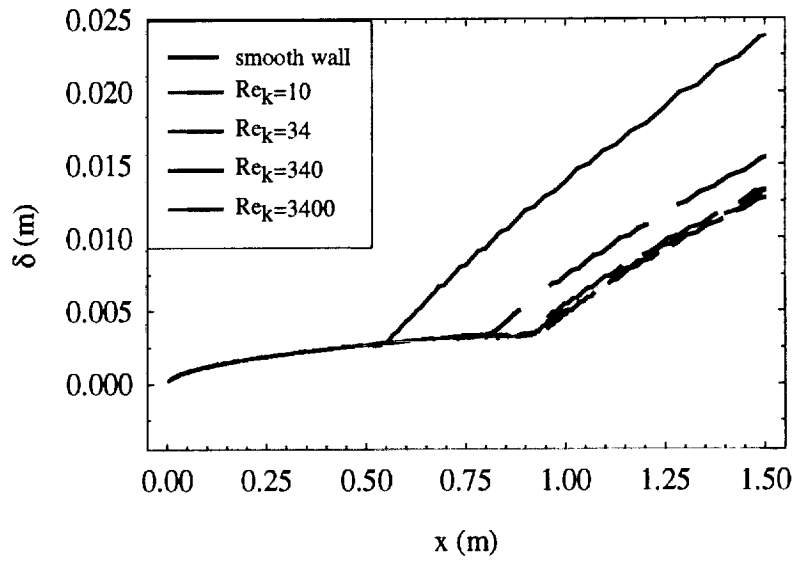
Year 1 Accomplishments

Flat Plate Model

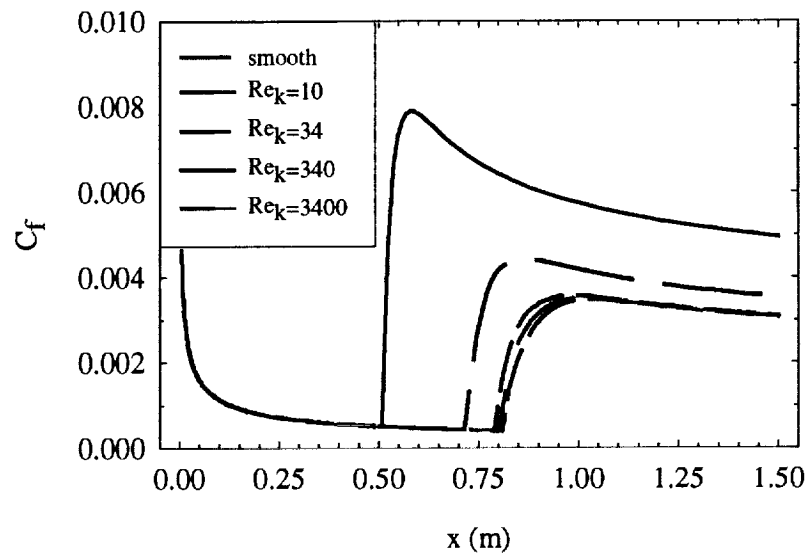
A flat plate test bed was required to accomplish these first-year goals. A new test section and flat plate were designed to produce a boundary layer where detailed measurements could be obtained. A boundary layer code EDDYBL (Wilcox, 1998) was used to predict the characteristics of the zero-pressure-gradient boundary layer that would be observed on this flat plate. The $k-\omega$ turbulence model was used so that the effects of roughness could be studied. The free-stream conditions are shown in the Table 1, and the predicted skin friction coefficient C_f and boundary-layer thickness δ for several different roughness values are shown in Figures 3 and 4. Figure 3 shows the results for natural transition, whereas Figure 4 shows the results for a tripped boundary layer. In both cases is evident that the boundary layer is sufficiently thick at the back of the plate (~1 cm) to make detailed boundary-layer measurements.

Table 1 - Freestream Values Used for Flat Plate Design.

U_∞	70 m/s	P_∞	75.3 kPa
ρ_∞	0.887 kg/m ³	Re_∞	$3.4 \times 10^6 / m$
T_∞	295.7 K	M	0.2

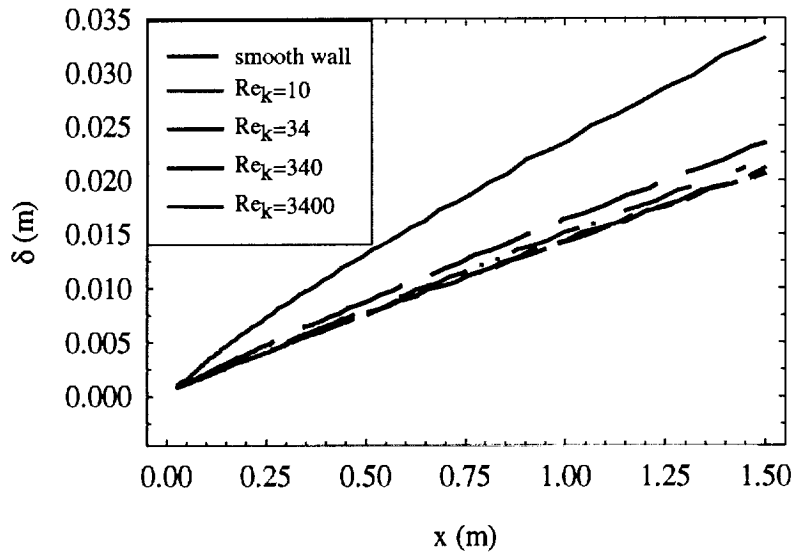


(a)

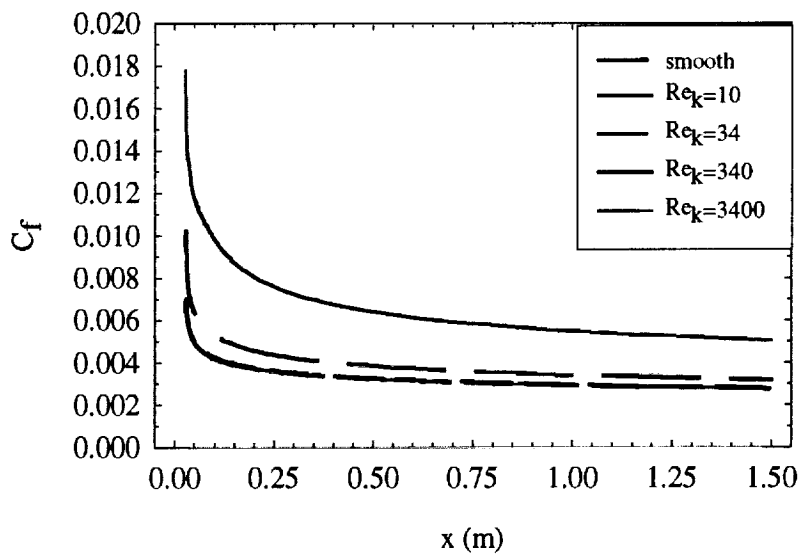


(b)

Figure 3 - Boundary layer parameters for a boundary layer with natural transition: (a) boundary-layer thickness, and (b) skin friction coefficient.



(a)



(b)

Figure 4 - Boundary layer parameters for a boundary layer tripped at the leading edge: (a) boundary-layer thickness, and (b) skin friction coefficient.

A flat plate model test bed has been built and is currently being tested in our subsonic wind tunnel. The 1.219 x 0.610 x 0.025 m flat plate, shown in Figure 5, has a frame construction that allows four interchangeable plates to make up the flat plate surface. This allows for plates incorporating different instrumentation or roughness to be quickly inserted. The plate has a 3:1 ellipse at the leading edge (see Figure 5(c)) to prevent separation and transition at the leading edge. To obtain the desired pressure gradient (zero for the preliminary work), the plate's angle of attack is controlled by changing the height of the support struts (See Figure 5(b)) at the front and rear of the model.

There are currently 20 different inserts that have been built for the flat plate model. Plates with instrumentation include a floating element balance, a plate with multiple pressure taps, and a highly polished stainless steel plate for oil-film interferometry C_f measurements (See Figure 6). The remaining plates will be coated with different levels of roughness to investigate its effect on the boundary layer.

Floating Element Balance

One of the most difficult aspects of the first year's work was the design and construction of the floating element balance. The balance is constrained to move in one direction so that it is only sensitive to shear stress in the stream-wise direction. A load cell measures the shear load applied to the floating element by the airflow.

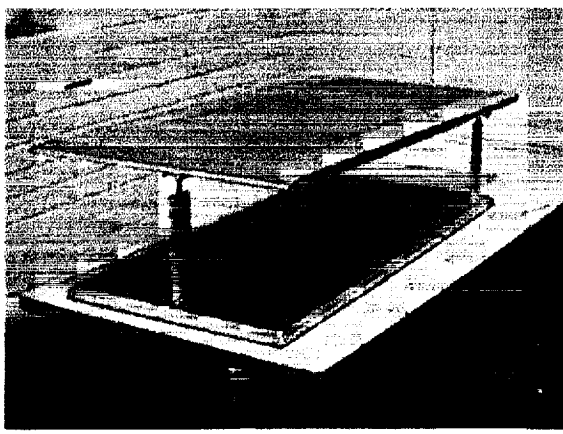
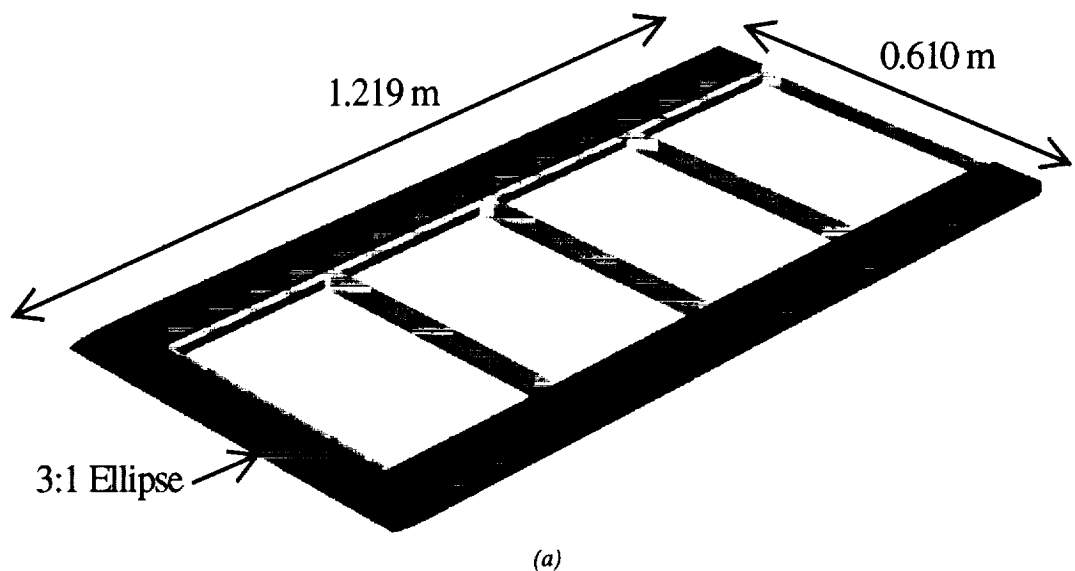
The balance consists of several parts. As shown in Figure 7(a) and (c), the sensitive element of the balance is a 33 x 12.7 cm cover plate. This cover plate is mounted to an undercarriage that is mounted to four linear bearings (not shown) that are rigidly attached to the fixed base of the balance. As a shear load is applied to the floating element in the direction shown in Figure 7 (a), the force is transmitted by the undercarriage (Figure 7(b)) to the load cell (Entran ELG-H Load Sensor) via a small adjustable force transmission bar (Figure 7(d)). The excitation to and the signal from the load cell are transmitted to a signal-conditioning device (Entran PS30-A) via a quick-disconnect cable.

Preliminary calibration of the floating balance indicates that it provides a linear response for loads between 0 and 0.6 N, which correspond to shear stresses between 0 and 14 N/m². This range of shear stresses encompasses the values we expect to encounter on the plate.

Viscous Forebody Drag Measurements

Another goal for the first year was the development of a means to measure the viscous forebody drag on the surface of the vehicle. Several candidates were evaluated including distributed point measurement techniques and integrated measurement techniques. The most promising technique was one that uses a measurement of the boundary layer thickness to infer the integrated viscous drag using the incompressible law-of-the-wake.

This work was primarily carried out at NASA-Dryden with support from the University of Wyoming. In this technique, the boundary layer is measured using two Pitot tubes; one is fixed at a location and measures the impact pressure outside the boundary layer, and the other is a floating probe that may be moved within the boundary layer. By locating the floating probe at a position where it reads an impact pressure that is some specified fraction of the free stream value, the viscous drag may be determined. The relationship between this impact pressure ratio and the viscous drag was determined by integrating the law-of-the-wake across the boundary layer. Solutions applicable to smooth surfaces with pressure gradients and rough surfaces in the absence of pressure gradients have been determined. More detail of this procedure may be found in Whitmore et al (2000).



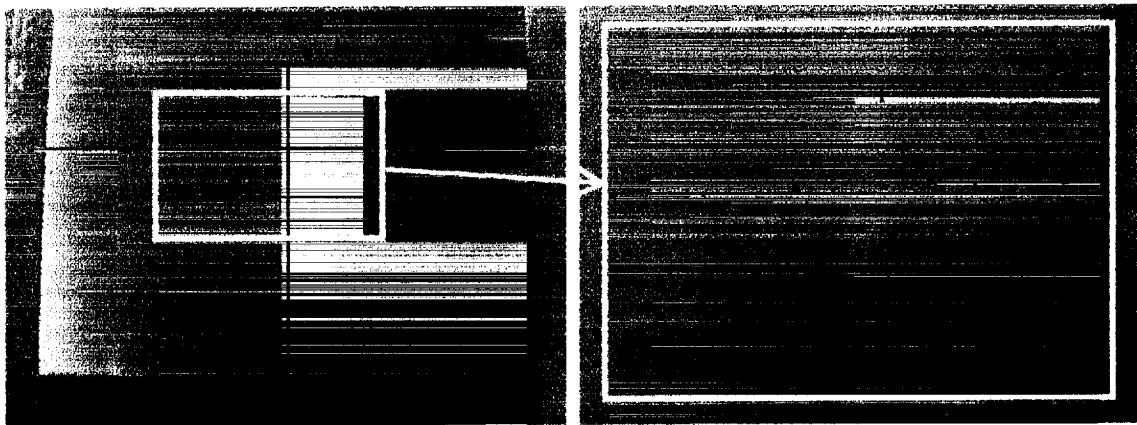
(b)

(c)

Figure 5 - Flat plate model: (a) schematic; (b) ready to be installed in test section; (c) leading edge detail.



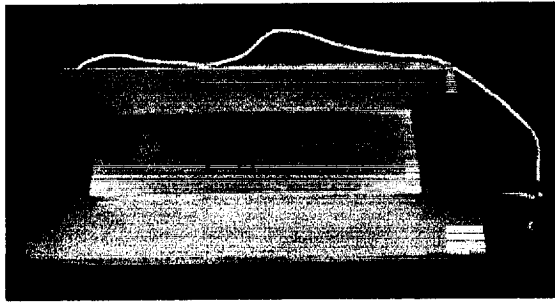
(a)



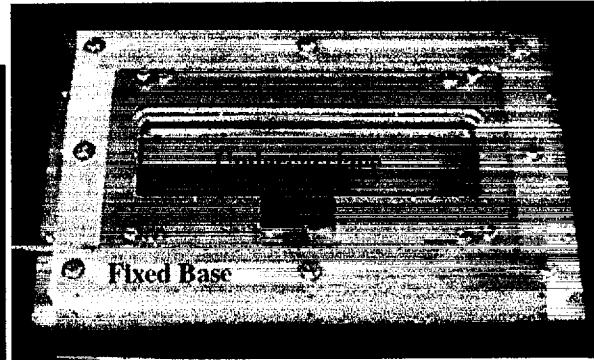
(b)

(c)

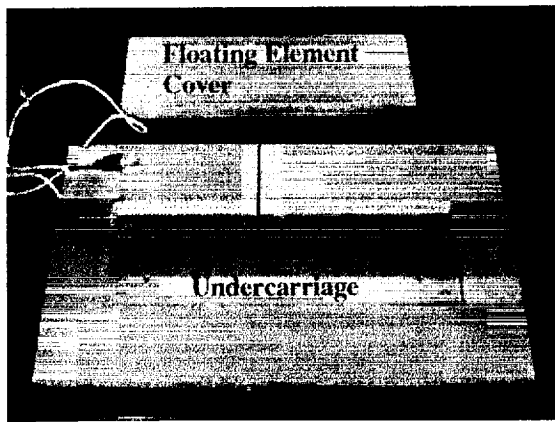
Figure 6 - Flat Plate Inserts: (a) oil-film interferometry plate - polished stainless reveals a reflection; (b) pressure tap plate - black lines indicate location of taps; and (c) close up of pressure taps.



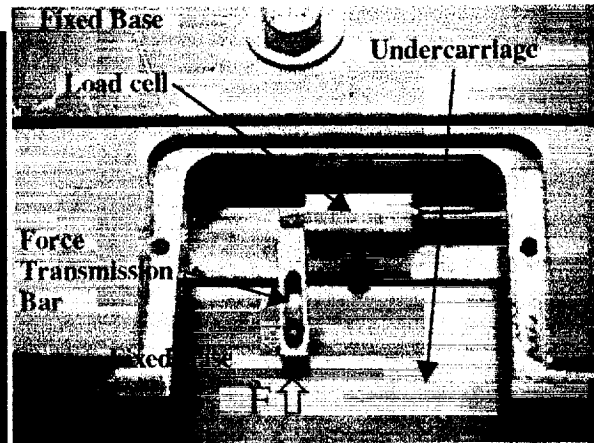
(a)



(b)



(c)



(d)

Figure 7 - Floating element balance insert: (a) Top view of assembled insert; (b) view of insert from underneath with protective cover removed; (c) Top view with element removed from sliding undercarriage; and (d) detail of load cell installation.

Planned Work

Currently, the flat plate is installed in the wind tunnel and preliminary measurements are taking place. Over the next several months, measurements of the shear stress distribution along the flat plate using oil-film interferometry, the floating element balance, and hot-wire surveys will be completed on both smooth and rough surfaces. These experiments will demonstrate our ability to make such measurements on rough surfaces and provide a detailed characterization of the flow over the flat plate.

Next year's work will focus on demonstrating the capability of measuring the integrated viscous drag using the dual-Pitot probe discussed above. In addition, Hoerner's curve in Figure 1 will be recreated in the controlled environment of the wind tunnel using ramps with different angles to produce a base area where the drag can be measured.

References

1. Hoerner, S.F., *Fluid Dynamic Drag*, Self-Published Work, Library of Congress Card no. 64-1966, Washington, DC, 1965, pp. 3-19, 3-20, 15-4, 16-5.
2. Saltzman, E.J., Wang, K.C., & Lliff, K.W., "Flight-Determined Subsonic Lift and Drag Characteristics of Seven Lifting-Body and Wing-Body Reentry Vehicle Configurations with Truncated bases," AIAA Paper 99-0383, 37th AIAA Aerospace Sciences Meeting, Reno, NV, January 1999.
3. Whitmore, S.A., & Moes, T.R., "A Base Drag Reduction Experiment on the X-33 Linear Aerospike SR-71 Experiment (LASRE) Flight Program," AIAA Paper 99-0277, 37th AIAA Aerospace Sciences Meeting, Reno, NV, January 1999.
4. Wilcox, D.C., *Turbulence modeling for CFD*, second edition, DCW Industries, La Canada, CA, 1998.
5. Whitmore, S.A., Hurtado, M., Rivera, J., & Naughton, J., "A Real-Time Method for Estimating Viscous Forebody Drag Coefficients," AIAA Paper 2000-0781, 38th AIAA Aerospace Sciences Meeting, Reno, NV, January 2000.

Publications from this Work

1. Whitmore, S.A., Hurtado, M., Rivera, J., & Naughton, J., "A Real-Time Method for Estimating Viscous Forebody Drag Coefficients," AIAA Paper 2000-0781, 38th AIAA Aerospace Sciences Meeting, Reno, NV, January 2000.